Optical spectra of ZnO in the far ultraviolet: First-principles calculations and ellipsometric measurements

Paola Gori,[1,2,6] Munise Rakel,[3] Christoph Cobet,[4] Wolfgang Richter,[5] Norbert Esser,[3,4] Axel Hoffmann,[3] Rodolfo Del Sole,[2,5,6] Antonio Cricenti,[1,6] and Olivia Pulci[2,5,6]

[1]*Consiglio Nazionale delle Ricerche, Istituto di Struttura della Materia, via Fosso del Cavaliere 100, 00133 Rome, Italy*

[2]*European Theoretical Spectroscopy Facility (ETSF), Rome, Italy*

[3]*Institut für Festkörperphysik, Technische Universität Berlin, 10623 Berlin, Germany*

[4]*Department Berlin, Institute for Analytical Sciences (ISAS), 12489 Berlin, Germany*

[5]*CNR-INFM-SMC, Dipartimento di Fisica, Università di "Tor Vergata," via della Ricerca Scientifica 1, 00133 Rome, Italy*

[6]*NAST, Rome, Italy*

(Received 16 December 2009; revised manuscript received 22 February 2010; published 19 March 2010)

We present ellipsometry data of the dielectric function of wurtzite ZnO in a wide energy range (2.5-32 eV). The ordinary and extraordinary components show a strong anisotropy above 10 eV, a feature for which ZnO deviates from the other II-VI wurtzite compounds. With the aid of *ab initio* calculations, performed within many-body perturbation theory (MBPT) and within time-dependent density-functional theory (TDDFT), we analyze the origin of the measured optical structures. TDDFT, with the use of a static long-range exchange-correlation kernel, proves to be a cheaper computational tool than MBPT to yield a good description of the whole spectrum. Theoretical results for the zinc-blende phase are also presented.

DOI: 10.1103/PhysRevB.81.125207 PACS number(s): 78.20.Ci, 71.15.Qe, 78.40.Fy

I. INTRODUCTION

ZnO (Ref. 1) is a wide and direct band gap (3.44 eV at low temperature[2]) II^B-VI semiconductor extensively studied for its applications in spintronics, piezoelectric devices, chemical sensors, and optoelectronics.[3] The latter are favored by an exciton binding energy of about 60 meV, which, being larger than room-temperature thermal energy (26 meV), allows efficient excitonic emission without the need of cooling devices. ZnO-based room-temperature polariton lasers emitting blue light can also be realized.[4] ZnO is explored as Ohmic contact for light emitters and photovoltaic solar cells because of its transparency at visible light.[5,6] Finally, the possibility of tailoring its attractive properties exploiting quantum-size effects makes ZnO a very promising material for nanostructures.[7,8]

We focus here on the optical response of bulk wurtzite (wz) ZnO, reporting ellipsometric measurements in the far UV. Ellipsometry allows a direct and reference-free determination of the whole set of linear optical functions by measuring the amplitude ratio of and the phase shift between parallel and perpendicular polarized components of the reflected light beam. Approximations in a subsequent Kramers-Kronig analysis to determine both the real and imaginary part of the dielectric function (DF), or n and k, are avoided. The use of synchrotron radiation supplies an intense polarized continuum spectrum of light in the whole range of electronic interband transitions in ZnO. Additionally, polarized light is very useful to study anisotropic properties with different orientation of the E vector to the optical axes. Most of the previous work is based on reflectance spectroscopy[9–11] which is not suitable to measure the phase shift. Limitation arises from the required extrapolation to the low and high photon energies, which are usually a dominant source of error. Another advantage of ellipsometry is the much lower sensitivity to scattering processes at *e. g.* defects or instabilities of the light source. Ellipsometry data for the UV range published so far are relatively rare[12,13] and still limited to energies below 10 eV. However, the main features (beside the free excitons close to the band gap) are expected in a range 10–18 eV due to the wide dispersion of valence bands including semicore Zn $3d$ levels. Furthermore, the origin of the strong anisotropy between the two independent tensor components parallel and perpendicular to the c axis in the higher energy region remained rather unattended.

In this paper, we present a joint study of calculated and measured optical spectra of wz ZnO in a wide energy range (2.5–20 eV). In the calculations, excitonic effects are included through the solution of the Bethe-Salpeter equation (BSE) (Ref. 14) and within the time-dependent density-functional theory (TDDFT) approach,[15] using the so-called "long-range kernel"[16] (LRK). TDDFT has been recently used to study the excited-state properties of ZnO molecules[17] and Zn_iO_i clusters[18] but has not been applied yet to bulk ZnO.

Theoretical results for zinc-blende (zb) ZnO, whose possible practical exploitation has been recently foreseen[19,20] because of high electron mobility and efficient p-type doping, are also presented.

II. COMPUTATIONAL APPROACH

The starting point of our calculations is density-functional theory[21] in the local density approximation (LDA).[22] We use a plane-wave code[23] and norm conserving pseudopotentials.[24] Regarding Zn, in particular, a pseudopotential (PP) in which all the electrons in the third shell ($3s^2 3p^6 3d^{10}$) are treated as valence states (Zn^{20+} PP) has been employed. It is well known, in fact, that neglecting the $3d$ states would produce an heavy underestimation of the lattice constants (≈18% in Ref. 25). The wave functions were expanded in-plane waves with a kinetic-energy cutoff of 240 Ry.

 ©2010 The American Physical Society

TABLE I. LDA and G_0W_0 gaps at high-symmetry points. G_0W_0NZ indicates $Z=1$. Energies are in eV. The experimental gap at Γ is 3.44 eV[2].

	Zn^{12+}			Zn^{20+}		
k point	LDA	G_0W_0	G_0W_0NZ	LDA	G_0W_0	G_0W_0NZ
Γ	0.81	0.8	0.8	0.74	2.6	3.1
A	3.93	4.3	4.4	3.85	6.0	6.6
H	9.46	10.6	10.9	9.30	11.9	12.5
K	9.55	10.5	10.7	9.34	11.5	12.1

Quasiparticle corrections to DFT-LDA eigenvalues have been calculated in the so-called G_0W_0 approximation,[26,27] as first-order perturbation to $\Sigma - V_{xc}$, where Σ is the self-energy and V_{xc} the LDA exchange and correlation potential. In this approximation, the self-energy is evaluated as $\Sigma = iG_0W_0$ with G_0, the single-particle Green's function, built through DFT wave functions and W_0, the screened Coulomb interaction, obtained in the random-phase approximation as $W_0 = \varepsilon^{-1} V$. A plasmon-pole model is employed for the frequency dependence of the dielectric function with 3858 plane waves and a mesh of $9\times9\times4$ k points in the Brillouin zone (BZ).[28] The resulting electronic gap at high-symmetry points, calculated with $3d$ (Zn^{12+}) and with $3d$, $3p$, $3s$ Zn semicore states (Zn^{20+}), are compared in Table I. Following Refs. 29 and 30, we have also performed a G_0W_0 calculation using $Z=1$, which means neglecting $\delta\Sigma/\delta E$ in the computation of the quasiparticle corrections (G_0W_0NZ in Table I). This approach has been shown to represent a way to include, at least in an approximated manner, self-consistency effects. The NZ results for a Zn^{20+} PP, shown in Table I, are in better accordance with the experiments, although the gap at Γ is still underestimated. Table I shows also that the inclusion of the full third shell of Zn (Zn^{20+} PP) is necessary to obtain acceptable results for the electronic gap, in contrast with the outcoming of the Zn^{12+} PP: when only the $3d$ semicore states are included, the G_0W_0 corrections are almost zero and an electronic gap at Γ as small as 0.8 eV (to be compared with an experimental gap of about 3.44 eV) is found. What mainly makes the case of Zn^{20+} different from the Zn^{12+} results is the overall increased exchange due to the new contribution between Zn $3d$ and Zn $3s$, $3p$ states.

Table II shows, instead, a few significant results for the gap at Γ obtained in literature using an all-electron approach,[31] hybrid functionals,[32–34] and B3LYP functionals.[35] Results obtained by partially self-consistent GW approaches, where the eigenvalues in G (Ref. 30) and in GW (Ref. 36) are updated, are also listed.

TABLE II. Calculated gap at Γ (eV) for wz ZnO.

Method	E_{gap}	Reference
AE+G_0W_0	2.44	Ref. 31
HSE	2.9	Ref. 32
HSE03+G_0W_0	3.2	Refs. 33 and 34
B3LYP	3.2	Ref. 35
LMTO+G_0W_0NZ off-diagonal	3.0	Ref. 30
LMTO+GW	3.64	Ref. 30
PAW+GW	3.2	Ref. 36

Partial self-consistency[36] improves the agreement with experiments. A GW calculation fully self-consistent on both the eigenfunctions and eigenvalues would probably be the most refined choice, without the need of using *ad hoc* parameters, as U or as the amount of exact exchange. But this approach would not be computationally feasible in our calculations of the optical properties of ZnO since thousands of k points (hence thousands of wave functions and thousands of GW corrections) are needed for well converged optical spectra.

Hence, we resorted to a compromise by using the best possible DFT-LDA wave functions (those calculated with the Zn^{20+} pseudopotential) and an average GW correction of 2.7 eV (scissor operator approximation) to match the gap at Γ. This value of the scissor is close to our G_0W_0NZ gap corrections averaged over the 4 high-symmetry k points in Table I (2.77 eV).

Optical spectra have been calculated in two ways: within many-body perturbation theory (MBPT) by solving the Bethe-Salpeter equation, and within the time-dependent DFT approach, using the long-range TDDFT f_{xc} kernel, $f_{xc} = -\alpha/q^2$, also known as LRK approach.[16] The solution of the BSE has been obtained by using Haydock's iterative method[37] to diagonalize the effective two-particle Hamiltonian in which the BSE is recast. 42 336 transitions (combining seven valence and seven conduction bands with a shifted mesh of $12\times12\times6$ k points in the BZ) have been included. It is known[38] that a huge amount of k points near Γ need to be included in order to accurately describe the free exciton, which has a binding energy of 60 meV. For good convergence of the spectrum at higher energy, instead, many less k points are needed. In particular, we have found that our set of k-points gives a reliable optical spectrum from 4 to 20 eV. For what concerns the TDDFT spectrum, instead, thanks to the fact that the computational load is less heavy, we could use more transitions (combining 16 valence and 8 conduction bands) and increase the number of k-points to $50\times50\times31$ k in the BZ, hence getting a much better convergence also in the low energy part of the spectrum.

III. EXPERIMENTAL

The ZnO samples are single crystals grown by the hydrothermal method provided by CrysTec. They are cleaved at

the a plane to achieve a surface normal along the $[11\bar{2}0]$ direction. With x-ray diffraction (XRD) measurements of the ω rocking curve we deduce a FWHM of 155.88 arcsec of the $(11\bar{2}0)$ reflection at $\omega=28.173°$. Raman spectroscopy reveals a E_2 (high) mode shift at 437.54 cm^{-1}. The orientation of the c axis in the surface plane was determined by reflectance anisotropy spectroscopy (RAS). The RAS determination of anisotropy is also very helpful to verify the ellipsometric data.[39]

All measurements were performed under ultrahigh-vacuum conditions (5×10^{-10} mbar) with a rotating analyzer ellipsometer by using a normal-incidence monochromator (beamline 3mNIM: 2.5–10 eV) and a toroidal grating monochromator (beamline TGM-4: 8–35 eV) at the Berliner Elektronenspeicherring-Gesellschaft für Synchrotronstrahlung (BESSY II). The polarization vector of the beam was tilted to 20° to the plane of incidence during the ellipsometric measurements. Actually, the high-energy limit depends on the reflectivity of the samples. Above the plasma edge of the material the reflectivity decreases rapidly and is fully utilized at nearly 32 eV for 45° angle of incidence.

The dielectric function was assessed with the assumption that the light is reflected at an ideal planar $[11\bar{2}0]$ surface (a plane) of the ZnO crystals. The effect of unintentional surface overlayers or surface roughness is assumed to be small. We have determined the so-called ellipsometric ratio ρ in two different azimuthal orientations with the c axis parallel (ρ_0) and perpendicular ($\rho_{\pi/2}$) to the plane of incidence. The two independent dielectric tensor components $\varepsilon_\perp$ and $\varepsilon_\parallel$ were finally calculated with two equations, which are deduced from the extended Fresnel relations for uniaxial anisotropic materials,[40]

$$\rho_0 = \left(\frac{\sqrt{\varepsilon_\perp\varepsilon_\parallel}\cos\phi_0 - \sqrt{\varepsilon_\perp - \sin^2\phi_0}}{\sqrt{\varepsilon_\perp\varepsilon_\parallel}\cos\phi_0 + \sqrt{\varepsilon_\perp - \sin^2\phi_0}}\right)\Big/\left(\frac{\cos\phi_0 - \sqrt{\varepsilon_\perp - \sin^2\phi_0}}{\cos\phi_0 + \sqrt{\varepsilon_\perp - \sin^2\phi_0}}\right) \tag{1}$$

and

$$\rho_{\pi/2} = \left(\frac{\varepsilon_\perp\cos\phi_0 - \sqrt{\varepsilon_\perp - \sin^2\phi_0}}{\varepsilon_\perp\cos\phi_0 + \sqrt{\varepsilon_\perp - \sin^2\phi_0}}\right)\Big/\left(\frac{\cos\phi_0 - \sqrt{\varepsilon_\parallel - \sin^2\phi_0}}{\cos\phi_0 + \sqrt{\varepsilon_\parallel - \sin^2\phi_0}}\right) \tag{2}$$

Figure 1 shows experimental real and imaginary parts ε_1 and ε_2 of the dielectric function of a-plane ZnO in the two polarizations parallel ($\varepsilon_\parallel$) and perpendicular ($\varepsilon_\perp$) to the optical c-axis measured at room temperature. In the band-gap region around 3.3 eV the spectra are dominated by strong excitonic absorption features (see inset). In $\varepsilon_\perp$ the A- and B-excitonic features could not be separated at this temperature and appear as one peak followed by a second broader peak related to their higher excitations to $n=2,3$ quantum states. The C exciton is observed in $\varepsilon_\parallel$.

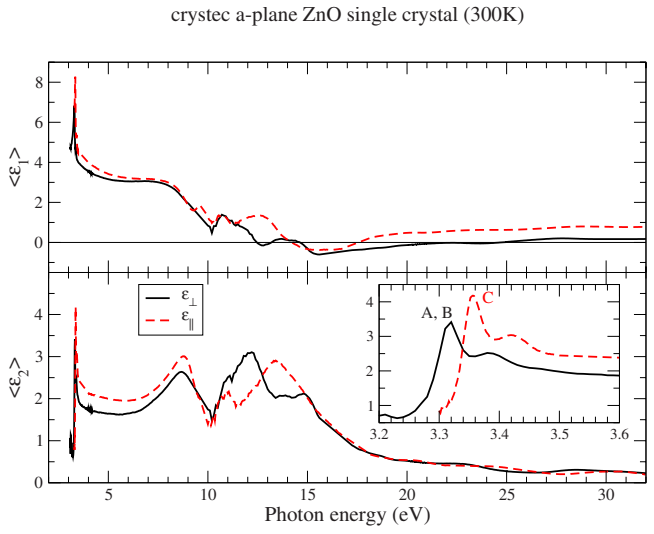

FIG. 1. (Color online) Room-temperature dielectric functions (real part: top panel; imaginary part: bottom panel) for wz ZnO measured for light polarized along the c axis (extraordinary component, dashed line) and perpendicular to the c axis (ordinary component, full line). Inset: Zoom of the absorption band edge displaying the free excitons A– C.

In the energy range of 4–7 eV no structures are observed and the anisotropy between extraordinary ($\varepsilon_\parallel$) and ordinary ($\varepsilon_\perp$) component in this region is weak. Also the broad structure in ε_2 at 7–9 eV shows a slight anisotropy. Finally, the structures at 12.0, 13.8, and 14.8 eV exhibit a very strong anisotropic behavior, which differs considerably from all other II-VI and wurtzite compounds,[41–43] where the main structures and anisotropy are found well below 12 eV.

IV. THEORETICAL RESULTS AND DISCUSSION

A. Electronic properties

The density of states (DOS), calculated at the G_0W_0NZ level using the Zn^{20+} PP, is shown in Fig. 2. The fully occupied Zn $3d$ semicore levels are centered at about −6.8 eV below the valence-band maximum, in reasonable agreement with photoemission data [−7.4 eV (Ref. 33)].

As seen from the DOS projected on the atomic orbitals (see inset of Fig. 2), and similarly to most binary semiconductors, the upper valence band of ZnO has a predominant

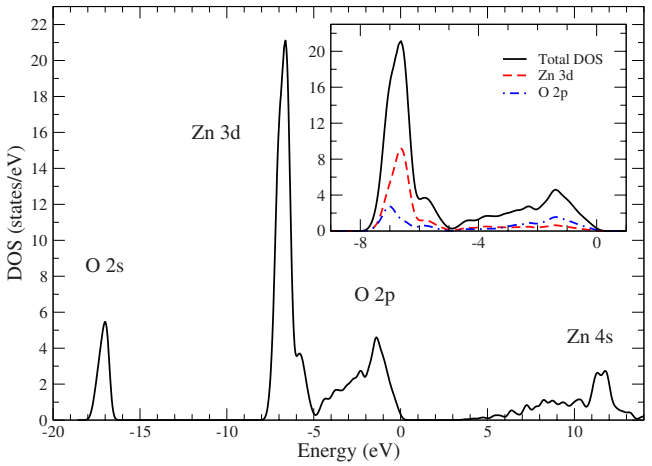

FIG. 2. (Color online) Calculated G_0W_0NZ DOS for wz ZnO. The inset shows the DOS projected on Zn 3*d* and O 2*p* orbitals.

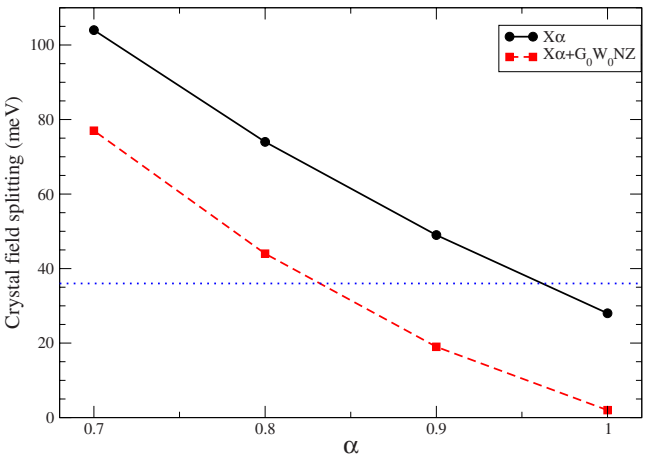

FIG. 3. (Color online) Crystal-field splitting as a function of the amount of local exchange within an $X\alpha$ (solid line) or $X\alpha + G_0W_0NZ$ approach (dashed line). The dotted line indicates our experimental value.

p-like character. Neglecting spin-orbit coupling and spin degrees of freedom, as it has been done in this work, the threefold degenerate upper valence band of a zinc-blende structure is split, in wurtzite, because of the symmetry lowering, into a singlet (Γ_1 state in the standard notation) and a doublet (Γ_5 states). The energy difference between these two states is the crystal-field splitting: $\Delta_{CF}=E(\Gamma_{5v})-E(\Gamma_{1v})$. This information, gained from LDA and *GW*-corrected band-structure calculations, is reported in Table III. The experimental value of this parameter is in the range 30–40 meV,[2,44] in agreement with our measured split between the (A,B) excitons and the C exciton (36 meV), as shown in the inset of Fig. 1. It appears that our calculated values of this parameter are either underestimated (Zn^{2+}) or overestimated (Zn^{12+}). Comparable values to the LDA-Zn^{12+} PP case have been obtained in literature in a projector augmented wave scheme, both in LDA and in GGA.[48] Also using a Zn^{20+} electronic configuration the crystal-field splitting is overestimated in LDA (106 meV) but in this case the *GW* corrections go in the right direction, indicating a more accurate description of the system with the latter PP.

We have then focused on the Zn^{20+} PP as starting electronic configuration. A few other results for the crystal-field splitting are reported in Table III. We can observe that both the G_0W_0 and the G_0W_0NZ approaches give an overestimation of the crystal-field splitting (about 80 meV), and even an update of the eigenvalues in the Green's function (G_1W_0) does not improve the situation. The fact that a Hartree-Fock calculation, instead, would provide a value of 54 meV, in better agreement with experiments, points towards the importance of the amount of exchange in the calculations. Following Lambrecht *et al.*,[45] we have then investigated the effect on the crystal-field splitting and on the position of the *d* bands caused by an artificial variation of the exchange functional. In particular, we have acted on the single-particle energies using a local exchange within the $X\alpha$ approximation,[46] with α ranging from 1 (corresponding to the Slater approximation) to 0.7. We find that increasing the amount of local exchange brings the *d* bands to higher binding energies, shifting them from about −5 eV in LDA to about −6.7 eV in the Slater approximation. Interestingly, the crystal-field splitting appears to decrease with increasing α, i.e., with increasing exchange, as shown in Fig. 3, solid line. Performing a G_0W_0NZ calculation on top of the $X\alpha$ electronic states, we find a systematic decrease of the crystal-field splitting (see Fig. 3, dashed line). For example, a G_0W_0NZ calculation on top of a $X\alpha$ (with $\alpha=0.8$) starting point would give a value for the crystal-field splitting of 44 meV, in acceptable agreement with the experimental range. The importance of the exchange on the crystal-field splitting

TABLE III. Calculated values of the crystal-field splitting (meV). $X\alpha$ values have been calculated using $\alpha=0.8$. Experimental values of the crystal-field splitting are 30 meV (Ref. 44), 40 meV (Ref. 2) and 36 meV (this work).

PP	LDA	G_0W_0	G_0W_0NZ	G_1W_0	HF
Zn^{2+}	8	2			
Zn^{12+}	105	207			
Zn^{20+}	106	83	77	85	54

	$X\alpha$	G_0W_0	G_0W_0NZ
Zn^{20+}	74	49	44

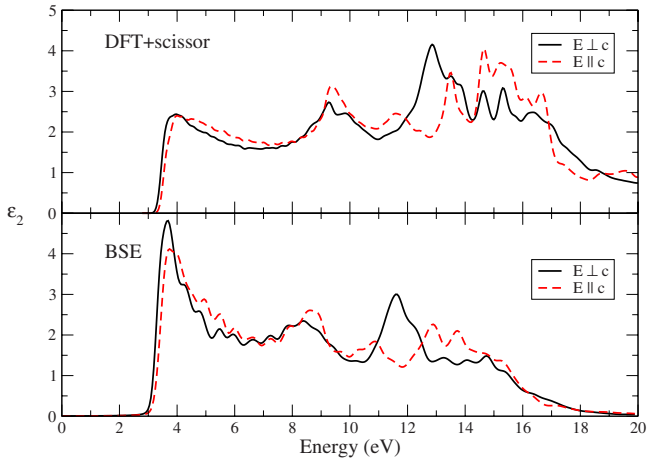

FIG. 4. (Color online) Imaginary part of the dielectric function of wz ZnO calculated at the DFT-RPA level plus scissor operator (upper panel) and at the BSE level (lower panel). The ordinary component is in full line and the extraordinary component in dashed line.

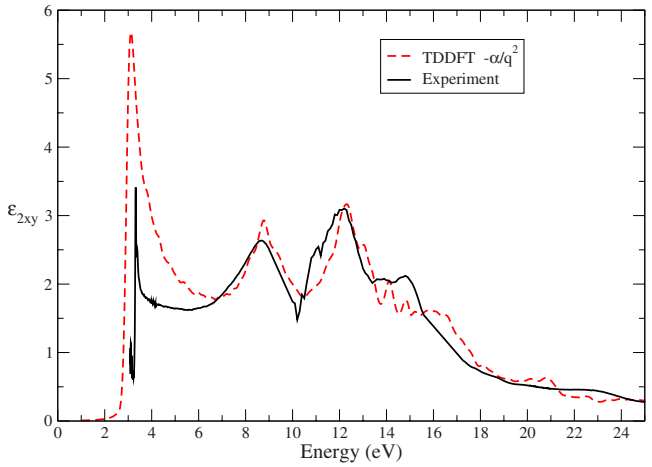

FIG. 5. (Color online) Experimental results for the ordinary component, compared with the TDDFT calculations.

was also found in Ref. 47, where a G_0W_0 calculation, on top of a hybrid functional HSE03 starting point, provides a crystal-field splitting of 54 meV.

B. Optical properties

Calculations of the dielectric function of wz ZnO have already appeared in literature: the dielectric function has been determined through *ab initio* calculations within DFT using different pseudopotential schemes: LDA (Ref. 49) or LDA+U,[50] GGA,[51,52] a screened exchange hybrid functional.[32] Excitonic effects in the optical properties have been included by solving the Bethe-Salpeter equation.[34,38,53]

Here, the imaginary part of the dielectric function ϵ_2 has been evaluated as a first step within the independent-particle picture with the Fermi golden rule (DFT-RPA, without local fields effects). A mesh of $50\times50\times31$ k-points has been used to sample the BZ and a broadening of 0.1 eV has been applied. The resulting spectra are shown in Fig. 4 (upper panel); a scissor operator shift of 2.7 eV has been applied to the DFT-RPA spectrum to match the experimental energy gap. It is clear that neglecting excitonic effects produces spectra slightly differing from the experimental ones in the positions of the optical structures but substantially differing in their intensities. In particular, the free excitons experimentally found around 3.4 eV, giving rise in Fig. 1 to a sharp peak, are of course not reproduced within a single-particle scheme.

As a second step, we have included excitonic effects within the BSE. The results of our calculations are shown in Fig. 4 (lower panel) for the ordinary and extraordinary component. The agreement with the experiments is greatly improved, although the excitonic peak is less sharp in our calculations, due to a limited number of k points we could use (864 in BZ). Our results are in good agreement with previous BSE calculations[34,53] and improve the description of the free exciton peaks compared to Ref. 38. The high-energy part of the calculated spectra shows a remarkably good agreement with the experiments also for what concerns the anisotropy of the dielectric function, correctly reproduced within the BSE, with the ordinary component more intense than the extraordinary one around 12 eV and vice versa at higher energies.

The description of the optical properties of ZnO is strongly affected by the number of k points used. One of the major drawbacks of MBPT is the high computational cost. Even using iterative schemes (such as Haydock recursive algorithm[37]), the solution of the BSE for excitonic matrices exceeding 100.000×100.000 becomes prohibitive.

An attractive alternative to MBPT is given by TDDFT, which comes with a lower computational load. Since we are dealing here with an extended system, it is important to describe correctly the long-range tail of the (unknown) TDDFT kernel. For this reason, we used the LRK (Ref. 16) $-\alpha/q^2$. The true f_{xc} kernel is energy dependent. Using such a simplified and static model to describe both free and not free excitons is difficult. We found that an optimal value for α is given by $\alpha=0.6$. This value is compatible with a dielectric constant between 5 and 6,[54] intermediate between the zero-frequency (ε_0) value 8, which accounts also for phonon contribution to screening, and the high-frequency one (ε_∞), about 4, which accounts only for electron screening.[55] A partial contribution of phonons to the dynamical screening of the electron-hole interaction must indeed be considered in ZnO since the exciton binding energy and the LO phonon energy are almost equal, about 60 meV.[55] When the exciton binding energy is calculated within the Wannier model, an effective dielectric constant $\varepsilon_{\text{eff}}=6$ is generally used.[56] A theoretical estimation made according to Strinati's theory[57] of the dynamical BSE yields, using values appropriate for ZnO, an effective dielectric screening of 5.2, corresponding to $\alpha=0.67$, in good agreement with the value $\alpha=0.6$ that we have used in our calculations. The comparison with experimental data is reported in Figs. 5 and 6 for ordinary and extraordinary components, respectively.

The agreement between calculated and experimental results is good, both regarding peak positions and relative intensities. The fact that a static LRK-TDDFT approach well describes the dielectric function points to a limited influence

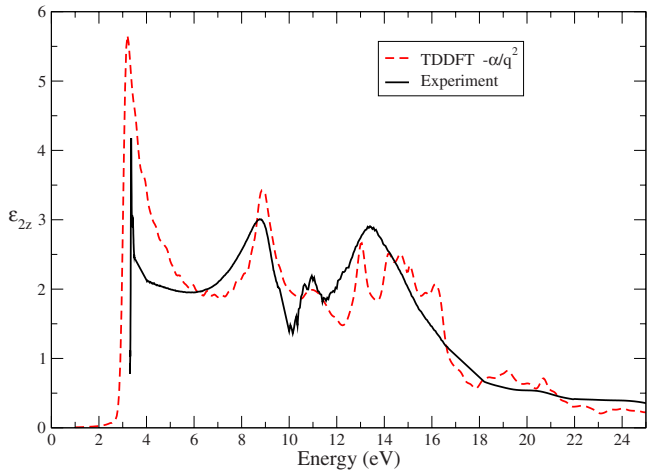

FIG. 6. (Color online) Experimental results for the extraordinary component, compared with the TDDFT calculations.

of excitonic effects in the high energy part of the spectrum. On the other hand, the possibility of using more k points within TDDFT leads to a description of the absorption line shape in the excitonic range better than in the BSE approach. An interpretation of the nature of the optical peaks can be done by analyzing the transitions that give rise to the imaginary part of the RPA dielectric function.

Regarding the ordinary component ($\varepsilon_\perp$), the first region after the absorption edge is mainly due to transitions at the Γ-point ($\Gamma_{5v} \rightarrow \Gamma_{1c}$). For the extraordinary component ($\varepsilon_\parallel$), the first region is similarly ascribed to the Γ-point, but the bands involved are $\Gamma_{1v} \rightarrow \Gamma_{1c}$ consistently with the selection rules that apply for wurtzite structures. The peaks found for both components at 8.8–8.9 eV are mainly due to transitions in the region between L and M from states located around −2 eV which have hybrid O 2p-Zn 3d character (see the inset in Fig. 2). The subsequent energy region is where the anisotropic character of the dielectric function is most evident. Regarding the ordinary component, the peak at 12.3 eV can be ascribed to the M point whereas the features between 14 and 15 eV are mainly due to transitions at Γ and at k points from Γ to A and originating from O 2p-Zn 3d states. The extraordinary component shows in this region two peaks: one at 11.0 eV, due to H_{3v}, $H_{1v,2v}$, and K_{3v}, K_{2v} contributions, and another at 13.0 eV, related to points of the BZ between L and H and between H and A. The broad structure in the extraordinary component located between 14 and 16.5 eV is dominated by transitions from Γ_{1v} to the second group of conduction bands.

C. Zinc-blende ZnO

The zinc-blende structure of ZnO is a metastable phase. It has been observed in ZnO epitaxially grown on GaAs(001) (Ref. 19) in ZnO films grown on Pt(111)/Ti/SiO_2/Si (Ref. 58) and, more recently, in tetrapods[59,60] and in nanoshells grown on ZnS nanoparticles.[20] Not many experimental data exist on this metastable phase. Optical absorption of zb-ZnO has not been measured yet, but several photoluminescence spectra have been published, showing a near-band-edge emission around 3.22–3.29 eV.[19,58,59]

TABLE IV. Calculated gap at Γ (eV) for zb-ZnO.

Method	E_{gap}	Reference
LDA+G_0W_0	2.2	This work
LDA+G_0W_0NZ	2.8	This work
LMTO-ASA+G_0W_0	3.59	Ref. 62
EXX+G_0W_0	3.11	Ref. 63

TEM images on tetragonally distorted ZnO/ZnS layers[19] bring to an estimated value for the lattice constant of 4.47 Å, and a value of 4.595 Å has been estimated by XRD measurements in ZnO films on Pt(111)/Ti/SiO_2/Si.[58]

In our calculations, a theoretical lattice constant of 4.56 Å is found, in the range of previous calculations[32] and in good agreement with the experiments. Our calculated electronic gap, which in DFT results 0.48 eV with Zn^{20+} PP, is corrected by quasiparticle (G_0W_0) effects[61] to 2.2 eV. Setting $Z=1$ (G_0W_0NZ in Table IV) increases the gap to 2.8 eV. Other GW calculations estimate the electronic gap to be 3.59 eV [LMTO+G_0W_0 (Ref. 62)] and, starting from and exact exchange calculation, 3.11 eV (Ref. 63) (see Table IV).

Optical spectra at the DFT, TDDFT, and BSE level are shown in Fig. 7. The BSE spectrum has been calculated using the Zn^{20+} pseudopotential, a grid of 2048 Chadi-Cohen shifted k points, seven valence bands and seven conductions bands. A scissor operator of 2.8 eV has been applied to all the spectra, in order to fit the theoretical gap with the experimental photoluminescence one. Important excitonic effects are clearly visible, also for this phase of ZnO, with a marked enhancement of the oscillator strength at the onset of the absorption. Comparison of the zb spectrum with the wz ones shows strong similarities, especially for the ordinary component.

V. CONCLUSIONS

The combination of first-principles calculations and experimental measurements of the dielectric tensor yields de-

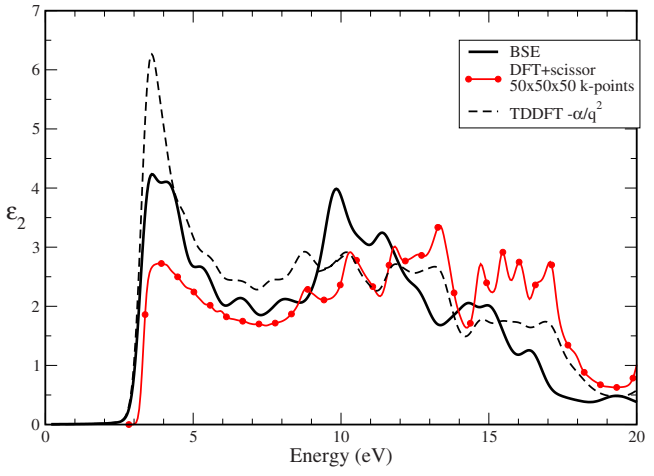

FIG. 7. (Color online) Imaginary part of the dielectric function calculated for zb-ZnO. The DFT plus a scissor operator shift, TDDFT and BSE results are compared.

tailed information about the electronic structure of ZnO. Distinct transition structures in the optical spectra have been assigned to certain critical points in the band structure and the origin of the anisotropy above 10 eV is found to be caused by the large hexagonal crystal field. At the band edge the anisotropy can only be reproduced when taking excitonic effects into account. The orbital resolved density of states shows considerable hybridization of the Zn 3*d* with the lower O 2*p* shell; hence, the *d* electrons strongly participate to the chemical bonding. The calculated overall frequency dependence of $\epsilon_{\perp}$ and $\epsilon_{\parallel}$ is in good agreement with the corresponding experimental values. Moreover, this work shows that TDDFT is a very suitable alternative to overcome the high computational cost of MBPT. Finally, the dielectric function for the rarely investigated case of the zinc-blende crystal structure is studied theoretically.

ACKNOWLEDGMENTS

We thank A. P. Seitsonen for useful discussions. The research leading to these results has received funding from the European Community's Seventh Framework Programme (Program No. FP7/2007-2013) under Grant Agreement No. 211956 (ETSF Project No. 121). CPU time granted by CINECA and ENEA-CRESCO, and their HPC teams support are gratefully acknowledged.

[1] For a review, see, for example, H. Morkoç and Ü. Özgür, *Zinc Oxide: Fundamentals, Materials and Device Technology* (WILEY-VCH Verlag GmbH & Co. KGaA, Weinheim, 2009).
[2] A. Mang, K. Reimann, and St. Rübenacke, Solid State Commun. **94**, 251 (1995).
[3] Ü. Özgür, Ya. I. Alivov, C. Liu, A. Teke, M. A. Reshchikov, S. Doğan, V. Avrutin, S.-J. Cho, and H. Morkoç, J. Appl. Phys. **98**, 041301 (2005).
[4] M. Zamfirescu, A. Kavokin, B. Gil, G. Malpuech, and M. Kaliteevski, Phys. Rev. B **65**, 161205(R) (2002).
[5] L. Stolt, J. Hedstrom, J. Kessler, M. Ruckh, K. O. Velthaus, and H. W. Schocki, Appl. Phys. Lett. **62**, 597 (1993).
[6] K. Ramanathan, M. A. Contreras, C. L. Perkins, S. Asher, F. S. Hasoon, J. Keane, D. Young, M. Romero, W. Metzger, R. Noufi, J. Ward, and A. Duda, Prog. Photovoltaics **11**, 225 (2003).
[7] Z. R. Tian, J. A. Voigt, J. Liu, B. McKenzie, M. J. McDermott, M. A. Rodriguez, H. Konishi, and H. Xu, Nature Mater. **2**, 821 (2003).
[8] L. Schmidt-Mende and J. L. MacManus-Driscoll, Mater. Today **10**, 40 (2007).
[9] R. Klucker, H. Nellkowski, Y. S. Park, M. Skibowski, and T. S. Wagner, Phys. Status Solidi B **45**, 265 (1971).
[10] R. L. Hengehold, R. J. Almassy, and F. L. Pedrotti, Phys. Rev. B **1**, 4784 (1970).
[11] J. L. Freeouf, Phys. Rev. B **7**, 3810 (1973).
[12] G. E. Jellison, Jr. and L. A. Boatner, Phys. Rev. B **58**, 3586 (1998).
[13] R. Schmidt-Grund, M. Schubert, B. Rheinländer, D. Fritsch, H. Schmidt, E. M. Kaidashev, M. Lorenz, C. M. Herzinger, and M. Grundmann, Thin Solid Films **455-456**, 500 (2004).
[14] For a review, see G. Onida, L. Reining, and A. Rubio, Rev. Mod. Phys. **74**, 601 (2002).
[15] E. Runge and E. K. U. Gross, Phys. Rev. Lett. **52**, 997 (1984); S. Botti, A. Schindlmayr, R. Del Sole, and L. Reining, Rep. Prog. Phys. **70**, 357 (2007).
[16] L. Reining, V. Olevano, A. Rubio, and G. Onida, Phys. Rev. Lett. **88**, 066404 (2002).
[17] B. Dai, K. Deng, J. Yang, and Q. Zhu, J. Chem. Phys. **118**, 9608 (2003).
[18] J. M. Matxain, J. M. Mercero, J. E. Fowler, and J. M. Ugalde, J. Am. Chem. Soc. **125**, 9494 (2003).
[19] For a review see, for example, A. Ashrafi and C. Jagadish, J. Appl. Phys. **102**, 071101 (2007), and references therein.
[20] M. V. Limaye, S. B. Singh, S. K. Date, R. S. Gholap, and S. K. Kulkarni, Mater. Res. Bull. **44**, 339 (2009).
[21] P. Hohenberg and W. Kohn, Phys. Rev. **136**, B864 (1964).
[22] W. Kohn and L. J. Sham, Phys. Rev. **140**, A1133 (1965).
[23] Calculations have been performed using the PWSCF code: S. Baroni, S. de Gironcoli, A. Dal Corso, and P. Giannozzi, http://www.pwscf.org/.
[24] N. Troullier and J. L. Martins, Phys. Rev. B **43**, 1993 (1991).
[25] P. Schröer, P. Kruger, and J. Pollmann, Phys. Rev. B **47**, 6971 (1993).
[26] M. S. Hybertsen and S. G. Louie, Phys. Rev. B **34**, 5390 (1986).
[27] R. W. Godby, M. Schlüter, and L. J. Sham, Phys. Rev. B **37**, 10159 (1988).
[28] The exchange part of Σ has been calculated using 16 985 plane waves; for the correlation part, we have used 3858 plane waves, 200 bands, 43 q vectors in $\varepsilon^{-1}(q,\omega)$.
[29] Y. M. Niquet and X. Gonze, Phys. Rev. B **70**, 245115 (2004).
[30] T. Kotani, M. van Schilfgaarde, and S. V. Faleev, Phys. Rev. B **76**, 165106 (2007).
[31] M. Usuda, N. Hamada, T. Kotani, and M. van Schilfgaarde, Phys. Rev. B **66**, 125101 (2002).
[32] J. Uddin and G. E. Scuseria, Phys. Rev. B **74**, 245115 (2006).
[33] A. R. H. Preston, B. J. Ruck, L. F. J. Piper, A. DeMasi, K. E. Smith, A. Schleife, F. Fuchs, F. Bechstedt, J. Chai, and S. M. Durbin, Phys. Rev. B **78**, 155114 (2008).
[34] A. Schleife, C. Rödl, F. Fuchs, J. Furthmüller, F. Bechstedt, P. H. Jefferson, T. D. Veal, C. F. McConville, L. F. Piper, A. DeMasi, K. E. Smith, H. Lösch, R. Goldhahn, C. Cobet, J. Zúñiga-Pérez, and V. Muñoz-Sanjosé, J. Korean Phys. Soc. **53**, 2811 (2008).
[35] J. Muscat, A. Wander, and N. M. Harrison, Chem. Phys. Lett. **342**, 397 (2001).
[36] M. Shishkin and G. Kresse, Phys. Rev. B **75**, 235102 (2007).
[37] L. X. Benedict, E. L. Shirley, and R. B. Bohn, Phys. Rev. B **57**, R9385 (1998); R. Haydock, Comput. Phys. Commun. **20**, 11 (1980).
[38] R. Laskowski and N. E. Christensen, Phys. Rev. B **73**, 045201 (2006).
[39] U. Rossow, R. Goldhahn, D. Fuhrmann, and A. Hangleiter, Phys. Status Solidi B **242**, 2617 (2005).
[40] R. M. A. Azzam and N. B. Bashara, *Ellipsometry and Polarized Light* (North-Holland Personal Library, New York, 1987).

[41] W. R. L. Lambrecht and M. Prikhodko, Solid State Commun. **121**, 549 (2002).
[42] C. Cobet, N. Esser, J. T. Zettler, W. Richter, P. Waltereit, O. Brandt, K. H. Ploog, S. Peters, N. V. Edwards, O. P. A. Lindquist, and M. Cardona, Phys. Rev. B **64**, 165203 (2001).
[43] C. Cobet, R. Goldhahn, W. Richter, and N. Esser, Phys. Status Solidi B **246**, 1440 (2009).
[44] B. Gil, A. Lusson, V. Sallet, S. A. Said-Hassani, R. Triboulet, and P. Bigenwald, Jpn. J. Appl. Phys. **40**, L1089 (2001).
[45] W. R. L. Lambrecht, A. V. Rodina, S. Limpijumnong, B. Segall, and B. K. Meyer, Phys. Rev. B **65**, 075207 (2002).
[46] J. C. Slater, Phys. Rev. **81**, 385 (1951).
[47] A. Schleife, C. Rödl, F. Fuchs, J. Furthmüller, and F. Bechstedt, Appl. Phys. Lett. **91**, 241915 (2007).
[48] S. Z. Karazhanov, P. Ravindran, A. Kjekshus, H. Fjellvåg, U. Grossner, and B. G. Svensson, J. Appl. Phys. **100**, 043709 (2006).
[49] Y. N. Xu and W. Y. Ching, Phys. Rev. B **48**, 4335 (1993).
[50] S. Z. Karazhanov, P. Ravindran, A. Kjekshus, H. Fjellvåg, and B. G. Svensson, Phys. Rev. B **75**, 155104 (2007).
[51] J. Sun, H. T. Wang, J. He, and Y. Tian, Phys. Rev. B **71**, 125132 (2005).
[52] A. Schleife, F. Fuchs, J. Furthmüller, and F. Bechstedt, Phys. Rev. B **73**, 245212 (2006).
[53] A. Schleife, C. Rödl, F. Fuchs, J. Furthmüller, and F. Bechstedt, Phys. Rev. B **80**, 035112 (2009).
[54] S. Botti, F. Sottile, N. Vast, V. Olevano, L. Reining, H.-C. Weissker, A. Rubio, G. Onida, R. Del Sole, and R. W. Godby, Phys. Rev. B **69**, 155112 (2004).
[55] H. Yoshikawa and S. Adachi, Jpn. J. Appl. Phys. **36**, 6237 (1997).
[56] K. Hümmer, Phys. Status Solidi B **56**, 249 (1973); J. Lagois, Phys. Rev. B **23**, 5511 (1981).
[57] G. C. Strinati, Phys. Rev. B **29**, 5718 (1984).
[58] S.-K. Kim, S.-Y. Jeong, and C.-R. Cho, Appl. Phys. Lett. **82**, 562 (2003).
[59] L. Lazzarini, G. Salviati, F. Fabbri, M. Zha, D. Calestani, A. Zappettini, T. Sekiguchi, and B. Dierre, ACS Nano **3**, 3158 (2009).
[60] Y. Wu, Y. Wu, X. H. Zhang, F. Xu, L. S. Zheng, and J. Kang, Nanotechnology **20**, 325709 (2009).
[61] In the calculation of ε^{-1} and of the correlation part of the self-energy, we have used 1687 plane waves and 500 bands, 10 Chadi-Cohen k points in the IBZ, and 19 q vectors. The exchange part of Σ has been calculated using 6975 plane waves.
[62] M. Oshikiri and F. Aryasetiawan, Phys. Rev. B **60**, 10754 (1999).
[63] P. Rinke, A. Qteish, J. Neugebauer, C. Freysoldt, and M. Scheffler, New J. Phys. **7**, 126 (2005).